Optimising microscopic spray characteristics and particle emissions in a dual-injection Spark Ignition (SI) engine by changing GDI injection pressure

Xiang Li [a, b, *], Dayou Li [b], Yiqiang Pei [a, *], Zhijun Peng [c, *]

[a] State Key Laboratory of Engines, Tianjin University, Tianjin, China

[b] School of Computer Science and Technology, University of Bedfordshire, Luton, UK

[c] School of Engineering, University of Lincoln, Lincoln, UK

*Corresponding author:

Xiang Li, School of Computer Science and Technology, University of Bedfordshire, Luton, LU1 3JU, UK

Email: xiang.li@beds.ac.uk

Yiqiang Pei, State Key Laboratory of Engines, Tianjin University, Tianjin, China.

Email: peiyq@tju.edu.cn

Zhijun Peng, School of Engineering, University of Lincoln, Lincoln, LN6 7TS, UK

Email: jpeng@lincoln.ac.uk

Abstract

Regarding reducing particle emissions from dual-injection spark ignition engines, most of the existing research focused on the benefits of using alcohol fuels. However, a comprehensive study of the effects of fuel injection pressure on microscopic spray characteristics and particle emissions in dual-injection spark ignition engines fuelled with gasoline has not been reported before. In this paper, with the assistance of phase Doppler particles analyser system and fast particle analyser, a study of optimising microscopic spray characteristics and particle emissions in a dual-injection spark ignition engine fuelled with gasoline by changing GDI injection pressure was conducted. The results show that by

increasing injection pressure from 5.5 MPa to 18 MPa, both normal and tangential components of droplet velocity increase, but the possibility of spray impingement would not increase a lot. Higher injection pressure would increase the probability of small droplets, and more droplets would collapse with a mode of continuous ripping or break down abruptly. From jet's central axis to sides, Sauter mean diameter increases first, then reduces outside the spray boundary. Increasing injection pressure from 5.5 MPa to 18 MPa reduces total particle number concentration, which is 53.98% and 45.44% at 2 bar and 10 bar, respectively. Meanwhile, the peak of particle number distribution curve decreases from 3.01×10^6 to 1.43×10^6 at 2 bar, whilst reducing from 1.08×10^6 to 5.33×10^5 at 10 bar. Overall, this paper comprehensively analyses the effects of fuel injection pressure on microscopic spray characteristics and particle emissions, whilst offering a practical approach to reduce particle emissions in dual-injection SI engines fuelled with gasoline.

Keywords

Dual-injection Spark Ignition (SI) engine; Particle emissions; Microscopic spray characteristics; Injection pressure

1. Introduction

Gasoline Direct Injection (GDI) engines have been a preferred selection by the automotive industry in recent years due to the advantages of improved fuel economy, transient response and power performance [1-8]. However, particles emitted by GDI engines not equipped with Gasoline Particulate Filter (GPF) are recognised higher than that of Port Fuel Injection (PFI) engines and some diesel engines with the Diesel Particulate Filter (DPF) [9-14].

Nowadays, particle emissions from vehicles powered by GDI engines negatively affecting air

quality and human health have attracted more attention from researchers [15][16]. The emission standards have also been more stringent for the restrictions of particle emissions [10][11][14]. In 2014, Euro 6b standard released and first limited the Particle Number (PN) emissions from vehicles powered by GDI engines to 6×10^{12}/km. Afterwards, it was further limited to 6×10^{11}/km by Euro 6c standard in 2017. To effectively reduce particle emissions of GDI engines, a dual-injection system was commercially applied as a novel technology by Toyota in 2005 [17]. As shown in Fig. 1, dual-injection Spark Ignition (SI) engines could offer combined advantages of PFI and DI as required, so it has been an effective way to reduce particle emissions.

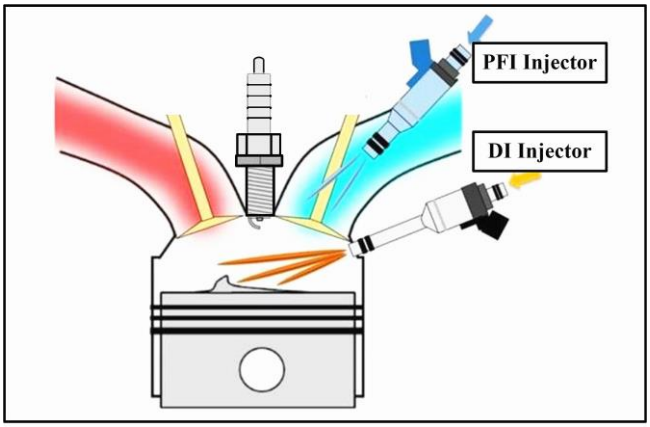

Fig. 1. Schematic of a dual-injection system in SI engine

Regarding the important research findings of particle emissions in dual-injection SI engines, Daniel et al. [18] concluded that the emission of large particles (> 50 nm) is almost removed by using ethanol fractions in dual-injection, resulting in a unimodal distribution of particle mass. Liu et al. [19][20] systematically compared the effects of "PFI-alcohols and DI-gasoline" and "PFI-gasoline and DI-alcohols" on PN reduction. It was indicated that as the alcohols mass ratio rises, PN would reduce more than 95% compared to pure gasoline DI injection. Moreover, under the selected engine operating conditions, there is an optimal mass fraction for PFI-alcohols to significantly reduce PN

66 and keep fuel economy and power performance in the meantime. Kim et al. [21] found that the size
67 distribution of particle moves to a smaller range when PFI-ethanol is added. The number reduction
68 of particles larger than 50 nm would bring a significant reduction in particle mass emissions. Catapano
69 et al. [22] demonstrated that due to the gaseous properties (no carbon-carbon bond), there is a benefit
70 of using Compressed Natural Gas (CNG) to reduce particle emissions in an optical CNG-gasoline
71 dual-fuel SI engine. Yu et al. [23] found that under the conditions of excess air ratio (λ) = 1 and 1.2,
72 the total PN emissions present an increasing trend with the increase of gasoline addition ratio.
73 Furthermore, due to improved fuel evaporation under lean-burn conditions, the accumulation mode
74 PN can remain at a low level. Kalwar et al. [24] found that the dual-fuel engine fuelled with
75 methanol/gasoline could achieve the lowest particle emissions among the fuel selections of
76 methanol/gasoline, ethanol/gasoline and butanol/gasoline. Liu et al. [25] demonstrated that when the
77 proportion of direct injection gasoline exceeds 50% in a PFI-ethanol and DI-gasoline dual-injection
78 engine, PN is strongly affected by the change of ignition timing or direct injection timing.

79 Regarding the particle emissions in dual-injection SI engines, it can be concluded that most of the
80 existing research focused on the benefits of using alcohol fuels, which is an effective way to reduce
81 particle emissions. However, in these cases, the lower heating value of alcohols as a disadvantage
82 should be considered, and the implementation of two fuel tanks and accessories would increase the
83 engine cost. Hence, it would make sense to further explore the potential of particle reduction in dual-
84 injection SI engines fuelled with gasoline.

85 Although the effects of injection pressure on particle emissions in SI engines has always been a
86 research hotspot in academia [26-33]. Wang et al. [26] demonstrated that increasing gasoline injection
87 pressure can help GDI engines reduce particle emissions. By a numerical study on a GDI engine,
88 Reddy et al. [28] found that there is an apparent decrease in the soot emissions with the increase of

injection pressure from 11 MPa to 20 MPa. Sharma et al. [29] concluded that injection pressure could significantly affect the air-fuel mixture preparation and particle emissions from a GDI engine fuelled with gasohol. By both simulation and experimental studies from a GDI engine fuelled with gasoline or bioethanol-gasoline blended fuels, Park et al. [30][31][33] demonstrated that increasing injection pressure is an effective way to reduce particle emissions, particularly under the wall wetting conditions. However, there is almost no study on the effects of injection pressure on particle emissions in dual-injection SI engines. Furthermore, a comprehensive study of the effects of fuel injection pressure on microscopic spray characteristics and particle emissions in dual-injection SI engines has not been reported before.

Therefore, a study of optimising microscopic spray characteristics and particle emissions in a dual-injection SI engine by changing GDI injection pressure up to 18 MPa was conducted in this paper. Although nowadays the maximum injection pressure of some latest generation engines has been improved to 35 MPa, the maximum injection pressure of 20 MPa is still one common option for commercialised GDI engines [26][28][32]. The findings of this paper would provide a deep understanding of the effects of fuel injection pressure on microscopic spray characteristics and particle emissions in dual-injection SI engines fuelled with gasoline, whilst offering a practical approach to the reduction of particle emissions. The rest of the paper is organised as follows: Section 2 mainly introduces the experimental setup of microscopic spray characteristics and engine testbed. Section 3 provides the experimental results and discussion, followed by the conclusions given in Section 4.

2. Experimental setup and procedure

2.1. Microscopic spray characteristics testbed and test procedure

The experiment of microscopic spray characteristics was conducted using a Phase Doppler

Particles Analyser (PDPA) system, as shown in Fig. 2. It mainly consists of an argon-ion laser, a beam separator, a transmitter, a receiver, a signal processor with 180 MHz frequency and a 3-D motion traverse system with high accuracy of 0.1 mm.

The GDI injector used in this study is from a dual-injection engine, which specifications are shown in Table 1. The orifice geometry and spray sketch of the five-hole injector are shown in Fig. 3. The information of the injector orifices is obtained from X-ray computed tomography, which indicates that the inner diameter of each hole is 0.174 mm. The fuel used in this study is commercial gasoline, which properties are shown in Table 2. The injector was installed in a customised metal holder, which fully kept the injector perpendicular to the ground and its position stability during the test. Fuel was injected into room conditions, which is 293 ± 0.5 K and 0.1 MPa. Fuel injection pressure was controlled and maintained with a high resolution of 0.1 MPa with the assistance of a high-pressure fuel pump. Besides, an air extraction hood was used to frequently extract the air out of the test site to eliminate the safety risks.

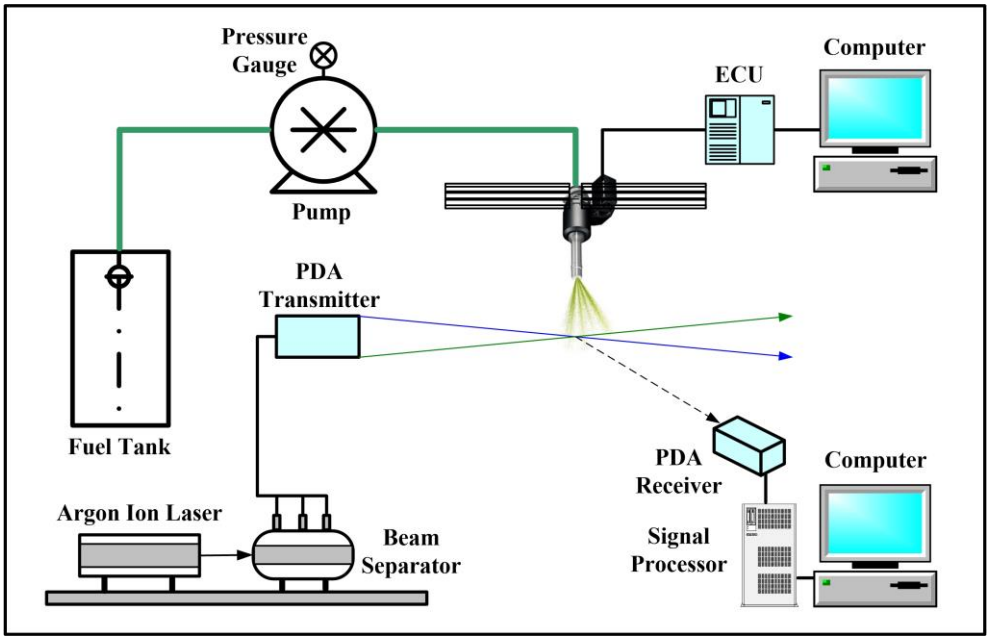

Fig. 2. Experimental setup of microscopic spray characteristic

Table 1. Engine specifications

Items	Content
Engine type	four-cylinder, four-stroke
Bore × Stroke (mm)	82.5 × 92
Displacement (L)	2.0
Injection type	Dual-injection system (PFI plus GDI)
Intake type	Turbocharged
Compression ratio	9.6:1
Rated speed (rpm)	5500
Rated power (kW)	160
Maximum Torque (N·m)	320

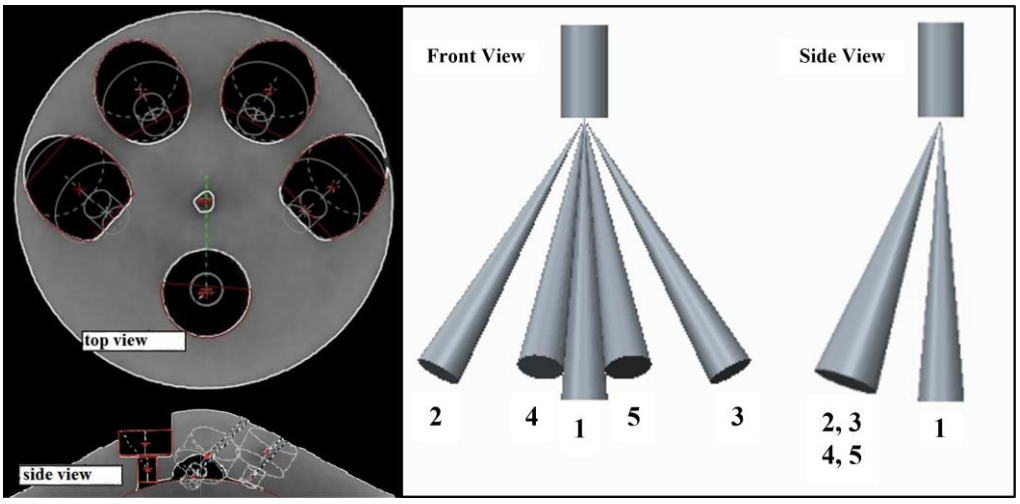

Fig. 3. Injector orifice geometry and spray sketch

Table 2. Fuel properties

Fuel type	Gasoline
Chemical formula	C5-C12
Relative molecular mass	95-120
Gravimetric oxygen content (%)	< 1
Research octane number	95
Density (20 ℃) (kg/L)	0.73
Dynamic viscosity (20 ℃) (mPa·s)	0.52
Kinematic viscosity (20 ℃) (mm^2/s)	0.71
Surface tension (20 ℃) (N/m)	22
Boiling range (℃)	30-200
Low heating value (kJ/kg)	44300
Latent heat of vaporisation (kJ/kg)	370

Laminar flame speed (20 ℃) (m/s)	0.33
Stoichiometric air-fuel ratio	14.7

In this research, fuel injection pressure was set to be 5.5 MPa, 10 MPa, 14 MPa and 18 MPa, covering the normal range of commercial GDI injection pressure. Based on the recommendation of the Society of Automotive Engineers (SAE) J2715, spray measurement points are typically 50 mm downstream along the injector axial direction [34]. Fig. 4 shows the coordinate system of measurement points during the test. The rightward and downward directions are defined to be the positive direction of "Y-axis" and "X-axis", respectively. For example, (4, 50) represents the point which is 4 mm right and 50 mm below the nozzle. Besides, the injector actuation signal was sent by a programmable Electronic Control Unit (ECU), which is also used to synchronise fuel injection with PDA data acquisition. During the test, laser wavelength of PDPA system ranged from 488 nm to 514.5 nm, and laser power was set to be 1.3 W. The measurement range of droplet velocity and size was -151.95 to 238.77 m/s and 0 to 236 μm, respectively. Meanwhile, the PDPA system can provide a high measuring accuracy, with resolutions of 0.01 m/s and 0.1 μm for droplet velocity and size, respectively. Furthermore, in order to avoid the interference of suspended fuel droplets, injection pulse width and injection frequency were set to be 1.2 ms and 0.1 Hz, respectively. To minimise the deviations by injection variations, data collection was completed with 20,000 validated sample droplets for each measurement point, and was repeated three times.

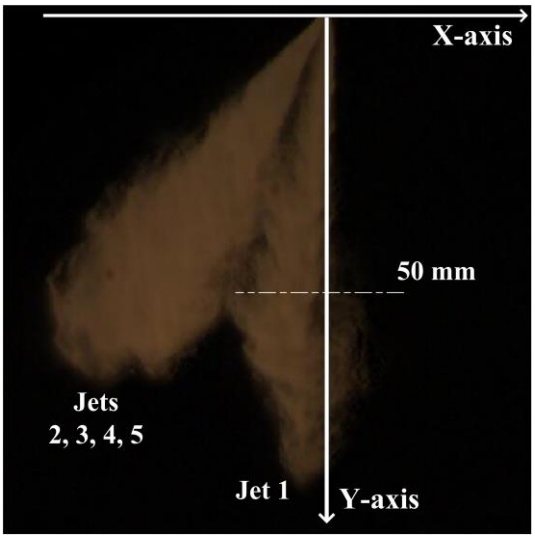

Fig. 4. Attached coordinate system of measurement points

In addition, some parameters used in the study of microscopic spray characteristics are introduced as follows. P_I denotes fuel injection pressure of GDI; t denotes the time After Start of fuel Injection (ASOI); V_N denotes normal component of droplet velocity; V_T denotes tangential component of droplet velocity; D_d denotes droplet diameter.

According to the research work by Arcoumanis et al. [35], droplets can be identified to be different regimes based on Weber number (We) which is commonly used to analyse the breakup mechanism, as shown in Equation (1).

$$We = \frac{\rho_l U^2 D_d}{\sigma} \tag{1}$$

Here, We denotes Weber number; ρ_l denotes fuel density; U denotes normal incident velocity; D_d denotes droplet diameter; σ denotes surface tension coefficient of the fuel.

As shown in Equation (2), droplets can be defined by Sauter Mean Diameter (SMD), which means the diameter of a sphere that has the same volume-surface area ratio as a droplet of investigation [36]. Based on the recommendation of SAE J2715, SMD is very effective to provide a better visual understanding for the diameter of a large cluster of droplets [34].

$$D_{SMD} = \frac{\int_{D_{min}}^{Dmax} D_d^3 dN}{\int_{D_{min}}^{Dmax} D_d^2 dN} \quad (2)$$

Here, D_{SMD} denotes SMD of droplet; D_d denotes droplet diameter; N denotes number of droplets.

2.2. Engine testbed and test procedure

Fig. 5 shows the schematic diagram of the engine testbed. An electrical dynamometer was coupled with a turbocharged dual-injection engine, which has been introduced in Table 1 before.

Piezo-electric spark-plug pressure sensors (AVL-GH13Z), a crank encoder (Kistler-2614CK1), a charge amplifier (Kistler-5018A) and a combustion analyser (AVL-641) were used to measure and analyse the transient in-cylinder pressure signals. A fast particle analyser (Cambustion-DMS 500) was connected to the exhaust pipe in front of the three-way catalytic converter to measure engine particle emissions, ranging from 5 nm to 1000 nm. In order to ensure the consistency of measurement standard for particle emissions under all conditions. The dilution factor of first-stage and second-stage in the particle analyser are kept at 1:4 and 1:100, respectively. In order to eliminate the impacts of cycle-to-cycle variations, cylinder pressure data were averaged by 200 consecutive cycles, and particle emissions data was measured three times for each measurement condition. The air-fuel equivalence ratio (lambda), intercooler outlet temperature and coolant kept constant at 1 ± 0.01, 298 ± 2 K and 360 ± 2 K, respectively. Besides, based on Holman's root mean square method [37], Table 3 presents that the uncertainties of the engine test are very low and completely acceptable.

In order to make the experimental procedure more efficient, the fuel mass ratio of PFI and GDI was kept at 1:1. Regarding the operating conditions, "2000 revolutions per minute (rpm)-2 bar Brake Mean Effective Pressure (BMEP)" and "2000 rpm-10 bar BMEP" were chosen to represent the engine typical low load and mid-high load, respectively. Meanwhile, a programmable ECU with software INCA can accurately control the GDI fuel injection pressure, spark timing and other operating

parameters. The spark timing was optimised to be the minimum advance for Maximum Brake Torque (MBT) or Knock Limited Spark Advance (KLSA). Besides, the engine speed, torque, stoichiometric air-fuel ratio and fuel injection timing are all kept constant under a fixed engine operating condition.

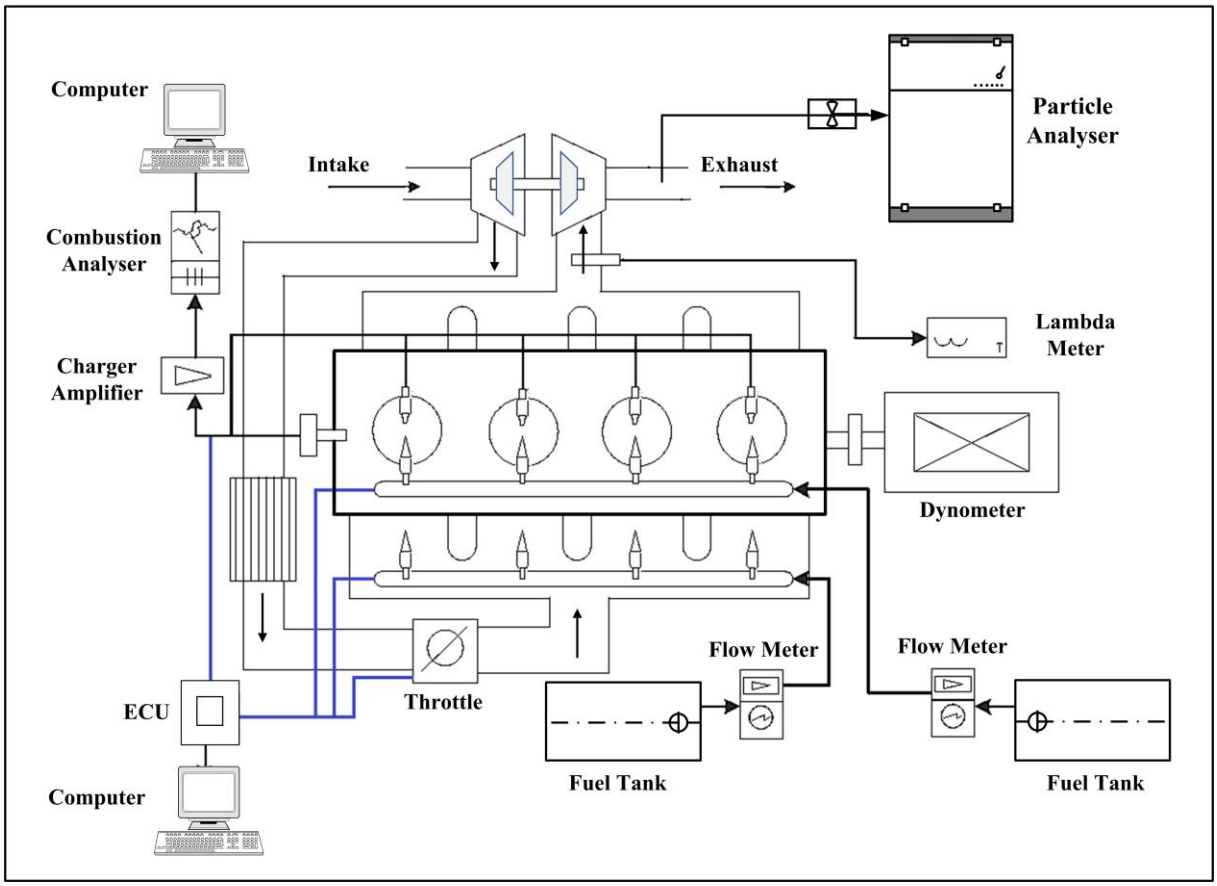

Fig. 5. Schematic diagram of engine testbed

Table 3. Uncertainties of measured parameters

Measured Parameters	Uncertainty (%)
Engine speed	± 0.1
BMEP	± 0.1
BSFC	± 0.2
Pressure	± 0.1
Crank angle	± 0.1
Lambda	± 0.3
Coolant temperature	± 0.4
Intercooler output temperature	± 0.4

Particle number	± 1.7

3. Results and discussion

3.1. Optimising microscopic spray characteristics by changing GDI injection pressure

Fig. 6 shows V_N at (0, 50) with varying P_I. It can be seen that when the tip of jet firstly reaches the measurement point, V_N is relatively high. Afterwards, V_N demonstrates a decline to a very low level. This is mainly because as time progresses, the spray would gradually collapse, reducing the regularity of droplets movement direction.

Besides, although V_N curves show similar overall trends under different P_I, but some discrepancies can also be observed. First, with the increase of P_I, V_N would be significantly improved. Under P_I = 18 MPa, V_N of spray tip can be up to around 42.5 m/s, which is much higher than the 30 m/s under P_I = 5 MPa. Second, the beginning of decline of V_N advances from 1.9 ms ASOI to 1.2 ms ASOI, leading to a shorter head section of V_N curve. Third, the decreasing rate of V_N curve would increase under higher P_I. These discrepancies can be mainly attributed to that by increasing P_I from 5.5 MPa to 18 MPa, the gap of the velocity between the jet surface and ambient gas would be enhanced. Hence, the increased instabilities for the droplets would have a negative impact on the kinetic energy of droplets movement along the axial direction. Therefore, it can be concluded that increasing P_I does not substantially increase V_N, which would not significantly raise the possibility of spray impingement.

Fig. 7 shows V_T at 50 mm of jet downstream. It can be seen that due to the interaction effects between adjacent plumes, the absolute value of V_T for measurement point (-16, 50) is a bit larger than (16, 50). With P_I increases from 5.5 MPa to 18 MPa, the absolute values of V_T shows a trend of increase. This can be attributed to that higher P_I increases the instability of spray, enhancing the tangential kinetic energy of droplets. Meantime, due to the stronger effects of vortex and interaction around the spray boundary, the increase of V_T becomes more obvious for the measurement points at

both ends. Consequently, with a higher P_I, both V_N and V_T of droplets increase, improving the diffusion rate of spray.

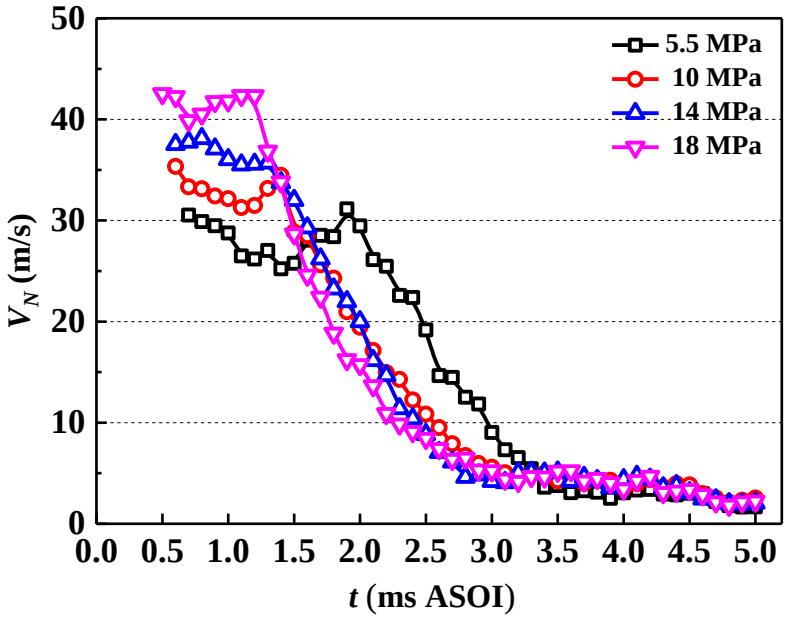

Fig. 6. V_N at (0, 50) with varying P_I

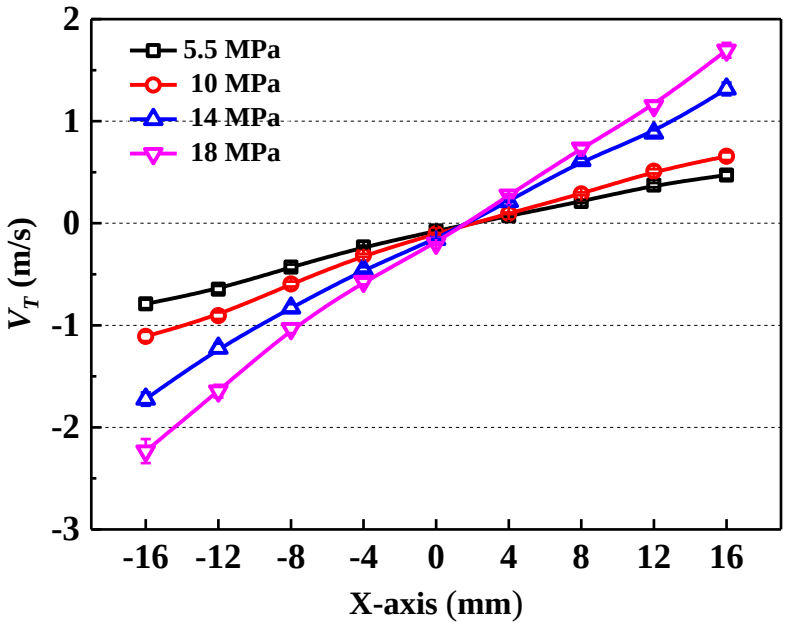

Fig. 7. V_T at 50 mm of jet downstream

Fig. 8 shows the probability of D_d with varying P_I. It shows that all the curves present unimodal

distributions. With the increase of P_I from 5.5 MPa to 18 MPa, the position of curve's peak moves from 10 μm to 6 μm. Moreover, the reduced probability of D_d larger than 20 μm can be found under P_I = 18 MPa. The higher probability of smaller D_d demonstrates that secondary atomisation of spray becomes more complete under higher P_I, which leads to a more homogeneous air-fuel mixture.

Fig. 9 presents the probability of droplet distribution at (0, 50) according to We. It shows that with the increase of P_I from 5.5 MPa to 18 MPa, the probability of droplets in the regime of "We < 100" has a reduction of 0.495%. The "We < 100" regime mainly includes vibrational and bag regimes, which represent that some droplets are deformed, shapeless or break into a number of fragments, but the breakup process is not very drastic compared to that of higher We droplets. In the meantime, the probability of droplets in "100 ≤ We < 1000" and "We ≥ 1000" increase by 0.482% and 0.013%, respectively. It means that more droplets would collapse with a mode of continuous ripping of the surface layer, even abruptly breaking down into a huge number of smaller and tiny droplets.

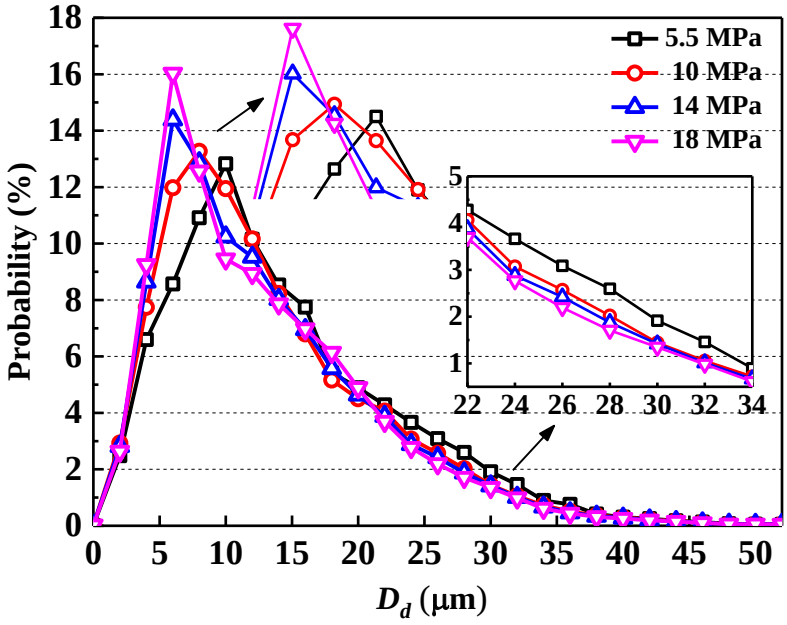

Fig. 8. Probability of D_d at (0, 50)

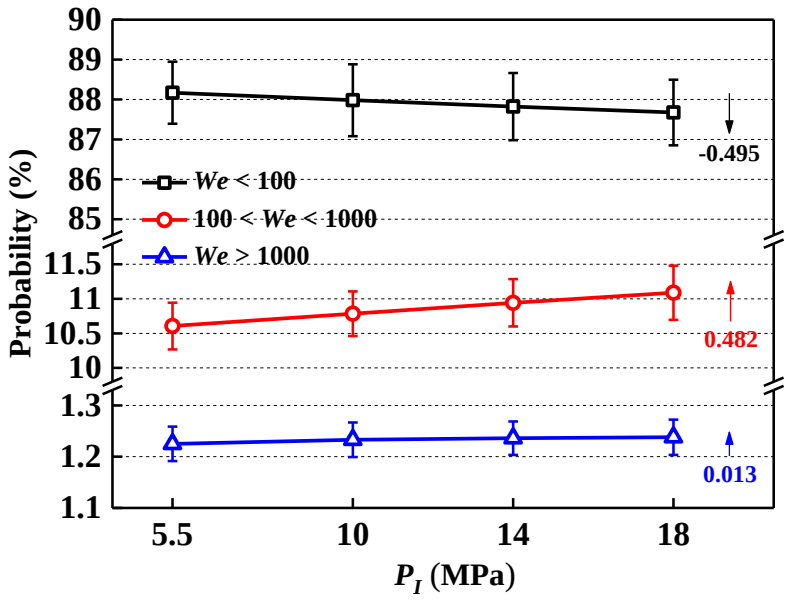

Fig. 9. Probability of droplet distribution at (0, 50) according to We

Fig. 10 presents D_{SMD} at 50 mm of jet downstream with varying P_I. It can be seen that regardless of P_I, all the curves present bimodal distribution. From jet's central axis to sides, D_{SMD} increases first by around 3 μm, then it has a reduction at both end measurement points (-16, 50) and (16, 50). This is because the probability of droplets collision and coalescence inside the spray boundary increases a lot, leading to an improvement in D_{SMD} [38][39][40]. However, the droplets outside the spray boundary are more affected by the shearing force between the jet surface and ambient gas, resulting in a higher possibility of breakup and a reduction in droplet size.

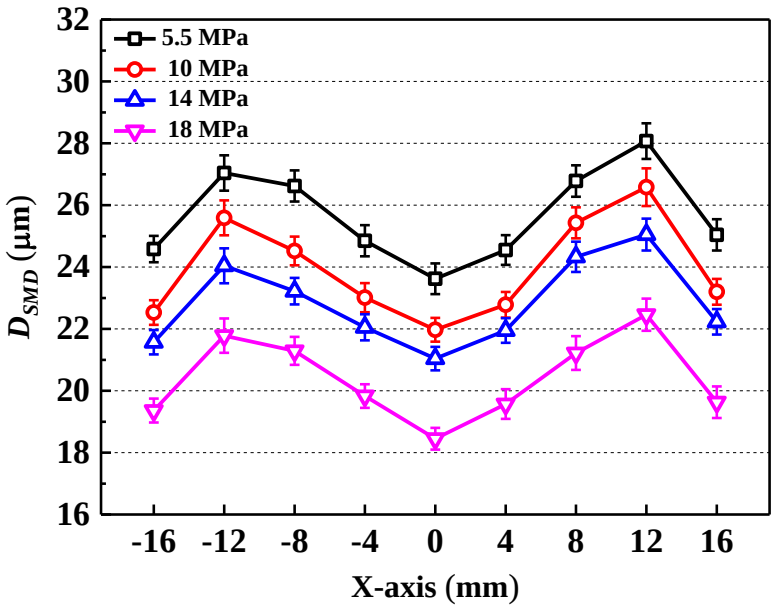

Fig. 10. D_{SMD} at 50 mm of jet downstream

3.2. Optimising engine particle emissions by changing GDI injection pressure

Based on the particle diameter (D_P) boundary of 30 nm to 50 nm, engine emitted particles can be classified into nucleation particle (5 nm $\leq$ D_P $<$ 30 nm) and accumulation particle (0 nm $\leq$ D_P $<$ 1000 nm) [41][42][43][44].

Fig. 11 shows the effects of P_I on PN concentration for nucleation, accumulation and total particles. A declining trend in particle emissions can be seen with the increase of P_I from 5.5 MPa to 18 MPa. The total PN concentration has a reduction of 53.98% and 45.44% at 2 bar and 10 bar, respectively. This is because the primary and secondary droplets atomisation can be accelerated, improving the homogeneity of air-fuel mixture. Moreover, the possibility of spray impingement would not increase a lot under a higher P_I, as stated in Section 3.1. Hence, PN concentration can be effectively restricted, as soot is generally formed as a by-product of incomplete combustion in fuel-rich mixture areas. Besides, because the impingement possibility is higher at 10 bar by the longer injection pulse, the decrease of PN concentration for accumulation and total particles at 10 bar is smaller than those of 2 bar.

These characteristics can be further explained by the effects of P_I on PN size distribution, engine

exhaust temperature (T_E) and maximum in-cylinder temperature (T_M).

Fig. 12 (a) shows all the PN curves present unimodal distributions at 2 bar. The curves mainly concentrate on the ultrafine particles ranging from 5 nm to 100 nm, and the peaks of curves centred around 15 nm.. Fig. 12 (b) shows that under 10 bar conditions, the PN curves present approximate bimodal distributions, which peaks are around 15 nm and 50 nm. By increasing of P_I to 18 MPa, the bimodal form becomes more obvious, as the reduction of accumulation PN is less than that of nucleation particles.

Fig. 12 also presents that with the increase of P_I, from 5.5 MPa to 18 MPa, the PN size distribution curves show a clear downward trend. The peak of the curve decreases from 3.01×10^6 to 1.43×10^6 at 2 bar, and reduces from 1.08×10^6 to 5.33×10^5 at 10 bar. This is mainly because of the benefits from the improved homogeneity of air-fuel mixture and higher in-cylinder temperature. As shown in Fig. 13, T_E and T_M have an increase of around 20 K and 60 K with the increase of P_I. With regards to reducing particle emissions, a higher temperature is usually helpful, which can be attributed to three factors. First, more complete combustion could decrease the production of particles from the development of unburned carbon elements. Second, the nucleation tendency of unburned hydrocarbon is potentially reduced. Third, the probability of particle oxidation can be increased, which could reverse the production of some particles.

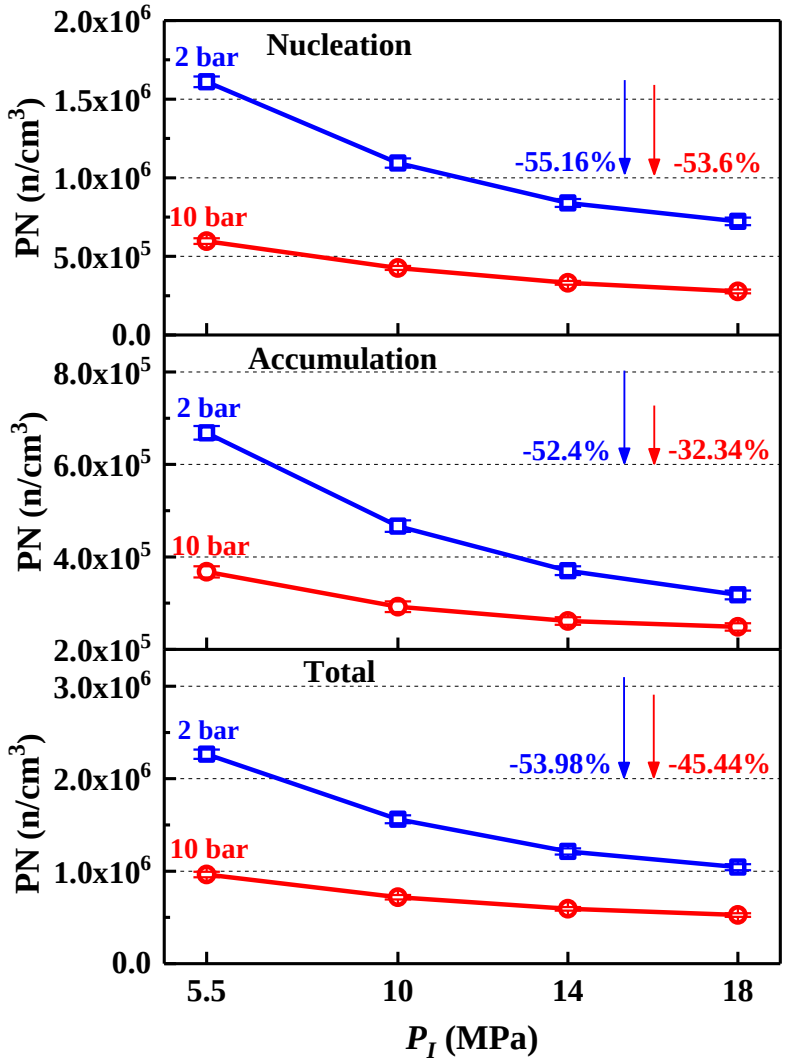

293

294 **Fig. 11.** Effects of P_I on PN concentration for nucleation, accumulation and total particles

295

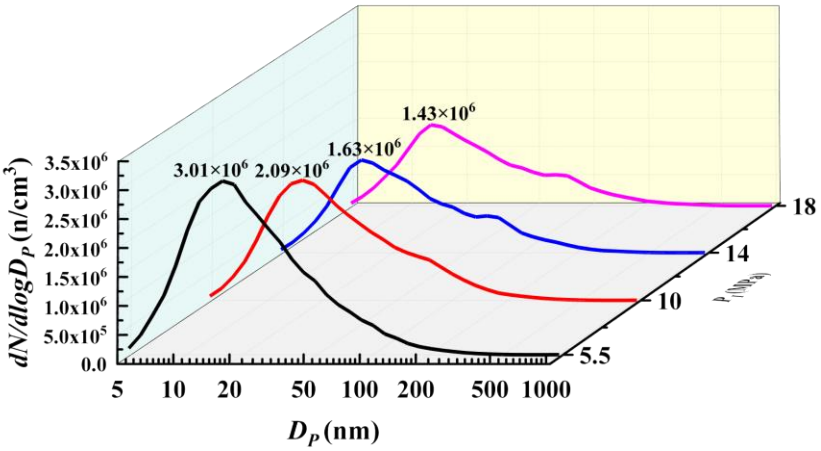

296

297 (a) 2 bar

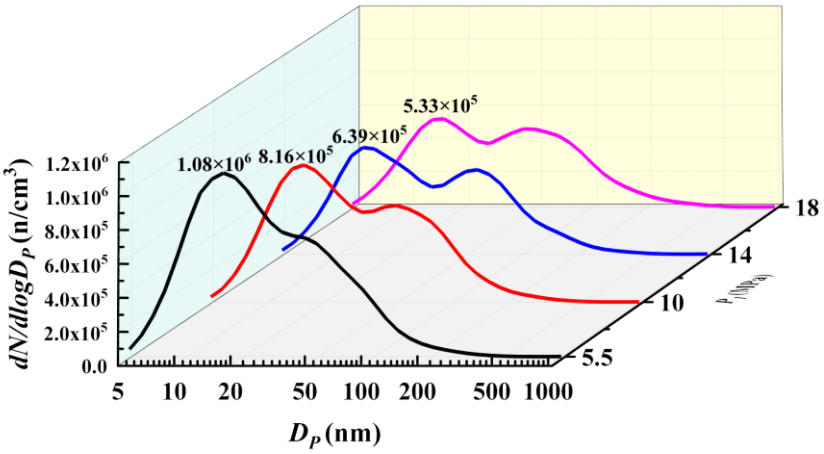

(b) 10 bar

Fig. 12. Effects of P_I on PN size distribution

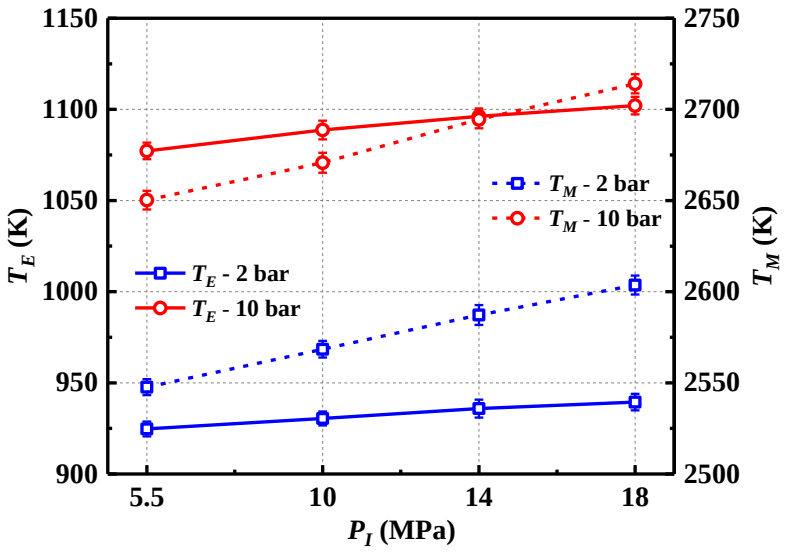

Fig. 13. Effects of P_I on T_E and T_M

4. Conclusions

The present study optimises the microscopic spray characteristics and particle emissions in a dual-injection SI engine fuelled with gasoline by changing GDI injection pressure. The study results not only present a comprehensive resource about the effects of injection pressure on microscopic spray characteristics and particle emissions, but also contribute to provide a practical approach to reduce particle emissions from dual-injection SI engines fuelled with conventional fuel (gasoline). The obtained results can be summarised as follows:

(1) With the increase of P_I from 5.5 MPa to 18 MPa, both V_N and V_T of droplets increase, which would enhance the diffusion of spray. However, the beginning of decline advances and the rate of decline increases. Hence, the possibility of spray impingement would not increase a lot under a higher P_I.

(2) By increasing P_I from 5.5 MPa to 18 MPa, the probability of smaller droplets is higher. The probability of droplets in the regime of "$We < 100$", "$100 \leq We < 1000$" and "$We \geq 1000$" have an increase of -0.495%, 0.482% and 0.013%, respectively. It is demonstrated that by increasing P_I, more droplets would collapse with a mode of continuous ripping or break down abruptly.

(3) From jet's central axis to sides, D_{SMD} increases first by around 3 μm, then reduces outside the spray boundary due to the strong shearing force between the jet surface and ambient gas.

(4) At 2000 rpm-2 bar, all the PN curves present unimodal distributions which peak most centred around 15 nm regardless of P_I. At 10 bar, PN curves present approximate bimodal distributions, which peaks are around 15 nm and 50 nm.

(5) By increasing P_I from 5.5 MPa to 18 MPa, T_E and T_M have an increase of around 20 K and 60 K. The peak of PN distribution curve decreases from 3.01×10^6 to 1.43×10^6 at 2 bar, whilst reducing from 1.08×10^6 to 5.33×10^5 at 10 bar. Correspondingly, total PN concentration significantly reduced 53.98% and 45.44% at 2 bar and 10 bar, respectively.

CRediT authorship contribution statement

Xiang Li: Conceptualization, Methodology, Software, Formal analysis, Investigation, Data curation, Visualization, Writing - original draft. **Dayou Li:** Writing - reviewing & editing. **Yiqiang Pei**: Methodology, Project administration, Funding acquisition. **Zhijun Peng:** Methodology, Writing

- reviewing & editing.

Declaration of Competing Interest

The authors declare that they have no known competing financial interests or personal relationships that could have appeared to influence the work reported in this paper.

Acknowledgement

This work is financially supported by the National Key Technology R&D Program of China (No. 2014BAG10B01).

Reference

[1] Gao Z, Li B, Li C, et al. Investigation on characteristics of ion current in a methanol direct-injection spark-ignition engine. Fuel, 2015, 141: 185-191.

[2] An Y, Pei Y, Qin J, et al. Development of a PAH (polycyclic aromatic hydrocarbon) formation model for gasoline surrogates and its application for GDI (gasoline direct injection) engine CFD (computational fluid dynamics) simulation. Energy, 2016, 94: 367-379.

[3] Li X, Pei Y, Qin J, et al. Effect of ultra-high injection pressure up to 50 MPa on macroscopic spray characteristics of a multi-hole gasoline direct injection injector fueled with ethanol. Proceedings of the Institution of Mechanical Engineers, Part D: Journal of Automobile Engineering, 2018, 232(8): 1092-1104.

[4] Raut A A, Mallikarjuna J M. Effects of direct water injection and injector configurations on performance and emission characteristics of a gasoline direct injection engine: A computational fluid dynamics analysis. International Journal of Engine Research, 2020, 21(8): 1520-1540.

[5] Han D, Fan Y, Sun Z, et al. Combustion and emissions of isomeric butanol/gasoline surrogates blends on an optical GDI engine. Fuel, 2020, 272: 117690.

[6] Raut A A, Mallikarjuna J M. Effect of in-cylinder air-water interaction on water evaporation and performance characteristics of a direct water injected GDI engine. Engineering Science and Technology, an International Journal, 2021, 24(2): 480-492.

[7] Li X, Peng Z, Ajmal T, et al. Simulation Study on Implementation of Oxy-Fuel Combustion for a Practical GDI Engine. SAE Technical Paper, 2021.

[8] Frommater S, Neumann J, Hasse C. A phenomenological modelling framework for particle emission simulation in a direct-injection gasoline engine. International Journal of Engine Research, 2021, 22(4): 1166-1179.

[9] Bonatesta F, Chiappetta E, La Rocca A. Part-load particulate matter from a GDI engine and the connection with combustion characteristics. Applied energy, 2014, 124: 366-376.
[10] Raza M, Chen L, Leach F, et al. A review of particulate number (PN) emissions from gasoline direct injection (GDI) engines and their control techniques. Energies, 2018, 11(6): 1417.
[11] Zhang M, Ge Y, Wang X, et al. Particulate emissions from direct-injection and combined-injection vehicles fueled with gasoline/ethanol match-blends–Effects of ethanol and aromatic compositions. Fuel, 2021, 302: 121010.
[12] Melaika M, Herbillon G, Dahlander P. Spark ignition engine performance, standard emissions and particulates using GDI, PFI-CNG and DI-CNG systems. Fuel, 2021, 293: 120454.
[13] Hu Z, Lu Z, Zhang H, et al. Effect of oxidation temperature on oxidation reactivity and nanostructure of particulate matter from a China VI GDI vehicle. Atmospheric Environment, 2021, 256: 118461.
[14] Huang Y, Surawski N C, Zhuang Y, et al. Dual injection: An effective and efficient technology to use renewable fuels in spark ignition engines. Renewable and Sustainable Energy Reviews, 2021, 143: 110921.
[15] Pope III C A, Ezzati M, Dockery D W. Fine-particulate air pollution and life expectancy in the United States. New England Journal of Medicine, 2009, 360(4): 376-386.
[16] Martins N R, Da Graca G C. Impact of PM2. 5 in indoor urban environments: A review. Sustainable Cities and Society, 2018, 42: 259-275.
[17] Ikoma T, Abe S, Sonoda Y, et al. Development of V-6 3.5-liter engine adopting new direct injection system. SAE Technical Paper, 2006.
[18] Daniel R, Xu H, Wang C, et al. Gaseous and particulate matter emissions of biofuel blends in dual-injection compared to direct-injection and port injection. Applied energy, 2013, 105: 252-261.
[19] Liu H, Wang Z, Long Y, et al. Comparative study on alcohol–gasoline and gasoline–alcohol Dual-Fuel Spark Ignition (DFSI) combustion for engine particle number (PN) reduction. Fuel, 2015, 159: 250-258.
[20] Liu H, Wang Z, Long Y, et al. Methanol-gasoline Dual-fuel Spark Ignition (DFSI) combustion with dual-injection for engine particle number (PN) reduction and fuel economy improvement. Energy, 2015, 89: 1010-1017.
[21] Kim N, Cho S, Min K. A study on the combustion and emission characteristics of an SI engine under full load conditions with ethanol port injection and gasoline direct injection. Fuel, 2015, 158: 725-732.
[22] Catapano F, Di Iorio S, Sementa P, et al. Particle formation and emissions in an optical small displacement SI engine dual fueled with CNG DI and gasoline PFI. SAE Technical Paper, 2017.
[23] Yu X, Guo Z, Sun P, et al. Investigation of combustion and emissions of an SI engine with ethanol port injection and gasoline direct injection under lean burn conditions. Energy, 2019, 189: 116231.
[24] Kalwar A, Singh A P, Agarwal A K. Utilization of primary alcohols in dual-fuel injection mode in a gasoline direct injection engine. Fuel, 2020, 276: 118068.
[25] Liu Z, Sun P, Du Y, et al. Improvement of combustion and emission by combined combustion of ethanol premix and gasoline direct injection in SI engine. Fuel, 2021, 292: 120403.
[26] Wang C, Xu H, Herreros J M, et al. Impact of fuel and injection system on particle emissions from a GDI engine. Applied Energy, 2014, 132: 178-191.
[27] Cho J, Si W, Jang W, et al. Impact of intermediate ethanol blends on particulate matter emission from a spark ignition direct injection (SIDI) engine. Applied Energy, 2015, 160: 592-602.

[28] Reddy A A, Mallikarjuna J M. Parametric study on a gasoline direct injection engine-A CFD analysis. SAE Technical Paper, 2017.
[29] Sharma N, Agarwal A K. Effect of the fuel injection pressure on particulate emissions from a gasohol (E15 and M15)-fueled gasoline direct injection engine. Energy & Fuels, 2017, 31(4): 4155-4164.
[30] Song J, Lee Z, Song J, et al. Effects of injection strategy and coolant temperature on hydrocarbon and particulate emissions from a gasoline direct injection engine with high pressure injection up to 50 MPa. Energy, 2018, 164: 512-522.
[31] Kim T, Song J, Park J, et al. Numerical and experimental study on effects of fuel injection timings on combustion and emission characteristics of a direct-injection spark-ignition gasoline engine with a 50 MPa fuel injection system. Applied Thermal Engineering, 2018, 144: 890-900.
[32] Choi Y, Lee J, Jang J, et al. Effects of fuel-injection systems on particle emission characteristics of gasoline vehicles. Atmospheric Environment, 2019, 217: 116941.
[33] Lee Z, Park S. Particulate and gaseous emissions from a direct-injection spark ignition engine fueled with bioethanol and gasoline blends at ultra-high injection pressure. Renewable Energy, 2020, 149: 80-90.
[34] Hung D L S, Harrington D L, Gandhi A H, et al. Gasoline fuel injector spray measurement and characterization–a new SAE J2715 recommended practice. SAE International Journal of Fuels and Lubricants, 2009, 1(1): 534-548.
[35] Arcoumanis C, Gavaises M, French B. Effect of fuel injection processes on the structure of diesel sprays. SAE transactions, 1997: 1025-1064.
[36] Wang D, Fan L S. Particle characterization and behavior relevant to fluidized bed combustion and gasification systems. Fluidized bed technologies for near-zero emission combustion and gasification. Woodhead Publishing, 2013: 42-76.
[37] Holman J P. Experimental methods for engineers. New York, NY: McGraw-Hill, 1966.
[38] Lacoste J, Crua C, Heikal M, et al. PDA characterisation of dense diesel sprays using a common-rail injection system. SAE transactions, 2003: 2074-2085.
[39] Wang Z, Xu H, Jiang C, et al. Experimental study on microscopic and macroscopic characteristics of diesel spray with split injection. Fuel, 2016, 174: 140-152.
[40] Wang Z, Guo H, Wang C, et al. Microscopic level study on the spray impingement process and characteristics. Applied Energy, 2017, 197: 114-123.
[41] Liu H, Li Z, Xu H, et al. Nucleation mode particle evolution in a gasoline direct injection engine with/without a three-way catalyst converter. Applied Energy, 2020, 259: 114211.
[42] Ma H, Jung H, Kittelson D B. Investigation of diesel nanoparticle nucleation mechanisms. Aerosol Science and Technology, 2008, 42(5): 335-342.
[43] Tan P, Ruan S, Hu Z, et al. Particle number emissions from a light-duty diesel engine with biodiesel fuels under transient-state operating conditions. Applied Energy, 2014, 113: 22-31.
[44] Masiol M, Harrison R M, Vu T V, et al. Sources of sub-micrometre particles near a major international airport. Atmospheric Chemistry and Physics, 2017, 17(20): 12379-12403.

Appendix

Abbreviations

ASOI	After Start of Injection
BMEP	Brake Mean Effective Pressure
CNG	Compressed Natural Gas
DPF	Diesel Particulate Filter
ECU	Electronic Control Unit
GDI	Gasoline Direct Injection
GPF	Gasoline Particulate Filter
KLSA	Knock Limited Spark Advance
MBT	Maximum Brake Torque
PDPA	Phase Doppler Particles Analyser
PFI	Port Fuel Injection
rpm	revolutions per minute
SAE	Society of Automotive Engineers
SI	Spark Ignition